THE JOURNAL OF BIOLOGICAL CHEMISTRY VOL. 288, NO. 5, pp. 3251–3264, February 1, 2013

N-Glycosylation-dependent Control of Functional Expression of Background Potassium Channels $K_{2P}3.1$ and $K_{2P}9.1$*[S]

Received for publication, July 30, 2012, and in revised form, December 11, 2012 Published, JBC Papers in Press, December 18, 2012, DOI 10.1074/jbc.M112.405167

Alexandra Mant[‡], Sarah Williams[‡1], Laura Roncoroni[‡1], Eleanor Lowry[§], Daniel Johnson[§], and Ita O'Kelly[‡2]

From the [‡]Human Development and Health, Centre for Human Development, Stem Cells and Regeneration, Faculty of Medicine, University of Southampton, Southampton SO16 6YD, United Kingdom and the [§]Faculty of Life Sciences, University of Manchester, Manchester M13 9PT, United Kingdom

Background: *N*-Glycosylation regulates the function of many membrane proteins.
Results: $K_{2P}3.1$ and $K_{2P}9.1$ possess functional glycosylation sites, and a lack of glycosylation results in fewer channels on the cell surface.
Conclusions: *N*-Linked glycosylation has a critical role in $K_{2P}3.1$ and a modulatory role in $K_{2P}9.1$ cell surface expression.
Significance: This defines a direct link between background potassium channel function and metabolic status.

Two-pore domain potassium (K_{2P}) channels play fundamental roles in cellular processes by enabling a constitutive leak of potassium from cells in which they are expressed, thus influencing cellular membrane potential and activity. Hence, regulation of these channels is of critical importance to cellular function. A key regulatory mechanism of K_{2P} channels is the control of their cell surface expression. Membrane protein delivery to and retrieval from the cell surface is controlled by their passage through the secretory and endocytic pathways, and post-translational modifications regulate their progression through these pathways. All but one of the K_{2P} channels possess consensus *N*-linked glycosylation sites, and here we demonstrate that the conserved putative *N*-glycosylation site in $K_{2P}3.1$ and $K_{2P}9.1$ is a glycan acceptor site. Patch clamp analysis revealed that disruption of channel glycosylation reduced $K_{2P}3.1$ current, and flow cytometry was instrumental in attributing this to a decreased number of channels on the cell surface. Similar findings were observed when cells were cultured in reduced glucose concentrations. Disruption of *N*-linked glycosylation has less of an effect on $K_{2P}9.1$, with a small reduction in number of channels on the surface observed, but no functional implications detected. Because nonglycosylated channels appear to pass through the secretory pathway in a manner comparable with glycosylated channels, the evidence presented here suggests that the decreased number of nonglycosylated $K_{2P}3.1$ channels on the cell surface may be due to their decreased stability.

Cellular membrane potential influences the function of both excitable and nonexcitable cells. The two-pore domain potassium (K_{2P}) channels are a family of background channels that regulate the membrane potential of cells in which they are expressed. Both structurally and functionally dissimilar to other potassium channel families, K_{2P} channels display little voltage or time dependence, are active at resting membrane potentials, and allow a constitutive leak of K^+ from cells (1, 2). The acid-sensitive K_{2P} subgroup (TASK channels) includes two well characterized members, $K_{2P}3.1$ (TASK-1) and $K_{2P}9.1$ (TASK-3), and a third proposed member ($K_{2P}15.1$ or TASK-5), which remains uncharacterized to date. Because of their cellular localization and sensitivity to physiological stimuli (extracellular acidification and hypoxia) TASK channels have been implicated in an array of physiological processes including regulatory roles in cell proliferation (and oncogenesis), activation of T-cells, chemoreception, and neuroprotective roles in response to ischemia and inflammation (3–5). TASK channels are also molecular targets for both local anesthetics and endocannabinoids (3, 6). These channels show constitutive activity once expressed on the cell surface; hence the control of TASK channel surface expression is of critical importance, because any change in channel number at the plasma membrane impacts the electrical properties of the cell in which these channels are expressed.

Numerous in-built processes within the secretory pathway are employed to regulate delivery of correctly folded membrane proteins, in appropriate number, to the cell surface. We and others have previously shown that TASK channel phosphorylation and association with cytosolic adaptor protein 14-3-3 is critical to $K_{2P}3.1$ and $K_{2P}9.1$ export from the endoplasmic reticulum (ER)[3] and hence cell surface expression (7–10).

Understanding of the quality control processes newly synthesized proteins undergo *en route* to the cell surface is still developing. Key steps include retention of nascent proteins within the ER until correctly folded and assembled, removal of persistently misfolded proteins, and transport of correctly folded proteins to the Golgi complex (GC). Further quality control together with protein maturation occurs within the endoplasmic reticulum-Golgi intermediate compartment (ERGIC)

* This work was supported by Biotechnology and Biological Sciences Research Council Grant BB/J008168/1 (to I. O.).
[S] This article contains supplemental Fig. S1.
[1] Supported by the Gerald Kerkut Charitable Trust.
[2] To whom correspondence should be addressed: Human Development and Health, Duthie Building, Mail Point 808, University of Southampton, Southampton SO16 6YD, UK. Tel.: 44-23-8079-6421; Fax: 44-23-8079-4264; E-mail: I.M.O'Kelly@southampton.ac.uk.

[3] The abbreviations used are: ER, endoplasmic reticulum; GC, Golgi complex; ERGIC, ER-golgi intermediate compartment; r, rat; MFI, mean fluorescence intensity; EEA1, early endosome antigen 1; HCN, hyperpolarization-activated cyclic nucleotide-gated; TASK, TWIK-related Acid Sensitive Potassium channels.

TABLE 1

Summary of K_{2P} constructs used in this study

Channels were tagged with eGFP fused to the N terminus, with or without an HA epitope tag in the external loop of the second pore-forming domain.

	Tag	Mutation	Experiments
K_{2P}3.1 rat channel			
$rK_{2P}3.1$	None	Wild type	Electrophysiology
$rK_{2P}3.1_{N53Q}$	None	N53Q	
GFP-$rK_{2P}3.1$	eGFP	Wild type	Immunofluorescence
GFP-$rK_{2P}3.1_{N53Q}$	eGFP	N53Q	
GFP-$rK_{2P}3.1$-HA	eGFP and HA	Wild type	Immunofluorescence, flow cytometry, and immunoblotting
GFP-$rK_{2P}3.1_{N53Q}$HA	eGFP and HA	N53Q	
K_{2P}9.1 rat channel			
$rK_{2P}9.1$	None	Wild type	Electrophysiology
$rK_{2P}9.1_{N53Q}$	None	N53Q	
GFP-$rK_{2P}9.1$	eGFP	Wild type	Immunofluorescence
GFP-$rK_{2P}9.1_{N53Q}$	eGFP	N53Q	
GFP-$rK_{2P}9.1$-HA	eGFP and HA	Wild type	Immunofluorescence, flow cytometry, and immunoblotting
GFP-$rK_{2P}9.1_{N53Q}$HA	eGFP and HA	N53Q	

and GC that ultimately leads to delivery of mature membrane proteins to the plasma membrane or removal of misfolded proteins to the endosomes and lysosomes (11, 12).

Protein glycosylation can play a key role in these processes and has previously been shown to be a critical modulator of ion channel gating, trafficking, and stability (13–16). *N*-Linked glycosylation occurs within the ER and undergoes further modifications within the GC (17). A large, preformed oligosaccharide precursor is added to the nascent protein within the ER. Trimming of specific glycans signals that the glycoprotein is ready for transport to the GC for further processing. If the glycosylated protein is unfolded or misfolded, a glucose residue is added back to the initial oligosaccharide, preventing its export to the GC (18, 19). Correct conformation of the protein triggers removal of this glucose residue and protein release from the ER. Similarly, within the GC, sugar moieties are rearranged. The final glycan composition and number regulates glycoprotein trafficking and stability (18, 20).

N-Glycosylation occurs on Asn in N*X*(S/T) motifs. Both $K_{2P}3.1$ and $K_{2P}9.1$ carry a conserved, predicted glycosylation site at position 53. We sought, therefore, to determine whether these channels are glycosylated *in vivo* and whether glycosylation has a regulatory role in channel function.

EXPERIMENTAL PROCEDURES

Molecular Biology—HA (YPYDVPDYA)-tagged rat (r) $K_{2P}3.1$ has been described previously (10). Similarly, the HA tag was introduced into GFP-$rK_{2P}9.1$ between Ala-213 and Leu-214, using *Pfu* Ultra DNA polymerase (Agilent Technologies UK Ltd., Stockport, UK). A conserved, putative glycosylated asparagine, Asn-53, was altered to glutamine in $rK_{2P}3.1$ and $rK_{2P}9.1$, GFP-$rK_{2P}3.1$, and GFP-$rK_{2P}9.1$ and the HA-tagged GFP-$rK_{2P}3.1$ and GFP-$rK_{2P}9.1$ (Table 1), also using *Pfu* Ultra DNA polymerase. The DNA constructs were fully sequenced before use.

Western Blotting—COS-7 cells were plated at 5×10^5 cells/10-cm dish in DMEM with 10% FCS and then transiently transfected with 10 μg of DNA encoding GFP-$rK_{2P}3.1$-HA, GFP-$rK_{2P}3.1_{N53Q}$HA, GFP-$rK_{2P}9.1$-HA, or GFP-$rK_{2P}9.1_{N53Q}$HA, using jetPEI transfection reagent, according to the supplier's instructions (Polyplus; Source Bioscience Autogen, Nottingham, UK). DNA-transfection complexes were removed from cells after 4 h and replaced with fresh DMEM with 10% FCS. Transfected cells were allowed to recover for 1 h, and then tunicamycin (or an equivalent volume of Me_2SO) was added to a final concentration of 1.0 μg/ml. Control and tunicamycin-treated samples were incubated for 16 h overnight at 37 °C, 5% CO_2. The cells were harvested by scraping on ice in PBS supplemented with a protease inhibitor mixture (Thermo Fisher Scientific and Perbio Science UK, Ltd., Cramlington, UK), washed in PBS, and then lysed for 30 min on ice in 200 μl of lysis buffer (10 mM Tris, pH 7.5, 150 mM NaCl, 0.5% Nonidet P-40) supplemented with protease inhibitors. The lysates were centrifuged at 5000 $\times$ *g* for 5 min at 4 °C, and the post-nuclear supernatant was mixed with protein sample buffer containing 100 mM DTT (final) for $K_{2P}9.1$ and 200 mM DTT (final) for $K_{2P}3.1$ and incubated for 30 min at room temperature. Samples were separated by SDS-PAGE and transferred to nitrocellulose membranes. The membranes were probed with either 1/1000 rabbit anti-GFP antibody (for $K_{2P}3.1$, ab290; Abcam, Cambridge, UK) or 1/1000 dilution anti-HA tag antibody (for $K_{2P}9.1$, mouse clone 16B12; Covance, Leeds, UK) and then a horseradish peroxidase-conjugated anti-rabbit or anti-mouse secondary antibody (Dako UK Ltd., Ely, UK), followed by detection using Pierce Super Signal West (Thermo Fisher Scientific).

Whole Cell Patch Clamping Recordings—HEK293 cells were plated on 22-mm sterile coverslips in 6-well plates at 10^5 cells/well. After 3 h, the cells were transiently transfected with either 1.5 μg of untagged, full-length $rK_{2P}3.1$ or $rK_{2P}3.1_{N53Q}$, or 0.1–0.25 μg of $rK_{2P}9.1$ or $rK_{2P}9.1_{N53Q}$ in pcDNA3.1 and 0.75 μg of eGFP-C1/well of a 6-well plate (Clontech), as described above. Controls were non-green fluorescent cells in the transfection wells.

Green fluorescent cells were selected for whole cell patch clamp analysis 24 h post-transfection. Pipette solution was K^+-rich and contained 150 mM KCl, 1 mM $MgCl_2$, 10 mM HEPES, 2 mM EGTA, pH 7.2, with KOH; free $[Ca^{2+}] = 27$ nM. Bath solution was Na^+-rich and contained 135 mM NaCl, 5 mM KCl, 1 mM $MgCl_2$, 10 mM HEPES, 1 mM $CaCl_2$, pH 7.8, with NaOH. All of the experiments were carried out at room temperature. Patch pipettes were manufactured from standard walled borosilicate glass capillary tubing (1B150-4; World Precision Instruments) on a two-stage Narishige PC-10 pipette puller (Narishige Scientific Instrument Laboratory, Kasuya, Tokyo, Japan), were heat-polished on a Narishige microforge, and had measured tip resistances of 2–5 MΩ (when filled with

K^+-rich pipette solution). Resistive feedback voltage clamp was achieved using an Axopatch 200 B amplifier (Axon Instruments, Foster City, CA). Voltage protocols were generated, and currents were recorded using Clampex 10.2 employing Digidata 1400A (Axon Instruments). The data were filtered (four-pole Bessel) at 1 kHz and digitized at 5 kHz. Following successful transition to the whole cell recording mode, capacitance transients were compensated for and measured. To evoke ionic currents voltage step protocol (−100 to 90 mV in 10 mV increments, 100 ms) was employed, and current-voltage relationships were constructed from the plateau stage of each 100-ms step.

Flow Cytometry—COS-7 cells were plated in 10 cm dishes, 5×10^5/dish and transfected transiently with 10 μg of plasmid DNA encoding GFP-rK_{2P}3.1-HA, GFP-r$K_{2P}3.1_{N53Q}$HA, eGFP alone, or empty pcDNA3.1 (Invitrogen), as described above. In tunicamycin-treated samples, the transfected cells were allowed to recover for 1 h before addition of the antibiotic (final concentration, 1.0, 0.1, or 0.01 μg/ml) or Me_2SO alone. After overnight incubation (16 h), the cells were harvested using trypsin and then stained at room temperature, with occasional gentle agitation, for 1 h with anti-HA tag antibody (Covance) at 1/400 dilution or an isotype control (IgG1; Invitrogen), followed by goat anti-mouse F(ab′)$_2$ fragment conjugated to Alexa Fluor 647 (Invitrogen; 1 h at room temperature; darkness; 1/1000 dilution). Immediately prior to analysis, the cells were stained with SYTOX AADvanced Dead Cell Stain (Invitrogen) to exclude damaged cells from the subsequent flow cytometric analyses (FACSCanto; BD Biosciences, Oxford, UK). Surface expression for each sample was calculated as the mean fluorescence intensity (MFI) of HA tag-stained cells minus the MFI of the corresponding isotype control. For low glucose experiments, COS-7 cells were grown in DMEM with 10% FCS containing 1 g/liter glucose ("low") or 4.5 g/liter glucose ("high") for 3–10 days, before transfection and analysis, as described above.

Microscopy—COS-7 cells were transfected transiently with DNA constructs encoding GFP-rK_{2P}3.1-HA, GFP-r$K_{2P}3.1_{N53Q}$HA, GFP-rK_{2P}9.1, or GFP-r$K_{2P}9.1_{N53Q}$ on coverslips as described above, cultured overnight, then fixed with 4% (w/v) formaldehyde in PBS for 7 min at room temperature, blocked with 3% (w/v) BSA in PBS, and stained with anti-HA tag antibody and goat anti-mouse F(ab′)$_2$ fragment conjugated to Alexa Fluor 647 or with biotinylated anti-mouse (Vector Laboratories, Burlingame, CA) and streptavidin-Texas Red (Vector Laboratories) as described above. For co-localization studies, fixed cells were permeabilized with 0.1% Triton-X-100 in PBS before the blocking step. The primary antibodies were mouse the anti-58-kDa Golgi protein (1/1000 dilution, clone 58K-9, Abcam), rabbit anti-ERGIC-53 (1/100 dilution, Sigma), and goat anti-EEA1 (1/100 dilution, C-15, Santa Cruz).

For the recycling assay, COS-7 cells were transfected transiently with GFP-rK_{2P}3.1-HA or GFP-r$K_{2P}3.1_{N53Q}$HA, cultured overnight, and then incubated for 2 h in DMEM without FCS. After 90 min, cycloheximide (Sigma) was added to a final concentration of 100 μg/ml. At 2 h, the cells were moved to a cold room (4 °C), placed on ice for 45 min, and then washed three times in ice-cold PBS. Surface proteins were biotinylated for 45 min on ice using 0.5 mg of EZ-Link NHS-SS-Biotin (Thermo Fisher Scientific) per well of a 6-well plate. The cells were then returned to DMEM with 10% FCS and 100 μg/ml cycloheximide and incubated for 0 and 20 min. At each time point, coverslips were transferred to wells containing ice-cold biotin stripping buffer (50 mM sodium methanethiolate, 50 mM Tris-HCl, pH 8.6, 100 mM NaCl, 1 mM $MgCl_2$, 0.1 mM $CaCl_2$), where they were incubated on ice for 15 min, the buffer was exchanged, and then the incubation was repeated. The stripping step was to remove noninternalized biotin from the plasma membrane. The coverslips were then rinsed with ice-cold PBS, fixed with 4% w/v formaldehyde as described above, and stained for EEA1 and biotin. Biotin was detected with a streptavidin-Alexa Fluor 546 conjugate (Invitrogen). Triple-stained vesicles were identified by drawing transects through regions of interest and looking for areas of signal overlap in all three dimensions. Quantitative analysis was carried out using Imaris 7.5.2 software. The coverslips were mounted and visualized using either a Zeiss Axio Observer D1 or using a Leica TCS SP5 confocal scanning microscope in the University of Southampton Biomedical Imaging Unit.

TABLE 2
Predicted N-glycosylation sites in K_{2P} channels

Protein sequences were analyzed using the NetNGlyc Server 1.0, hosted by the Center for Biological Sequence Analysis at the Danish Technical University.

Channel	Human	Mouse	Rat
K_{2P}1.1 (TWIK-1)	Asn-95	Asn-95	Asn-95
K_{2P}2.1 (TREK-1)	Asn-110	Asn-110	Asn-95
	Asn-134	Asn-134	Asn-119
K_{2P}3.1 (TASK-1)	Asn-53	Asn-53	Asn-53
K_{2P}4.1 (TRAAK)	Asn-78		
	Asn-82	Asn-81	Asn-81
K_{2P}5.1 (TASK-2)	Asn-77	Asn-77	Asn-77
K_{2P}6.1 (TWIK-2)	Asn-85	Asn-83	Asn-79
			Asn-85
K_{2P}7.1	Asn-83		Asn-83
K_{2P}9.1 (TASK-3)	Asn-53	Asn-53	Asn-53
K_{2P}10.1 (TREK-2)	Asn-144	Asn-144	
	Asn-148	Asn-148	
K_{2P}12.1 (THIK-2)	Asn-78	Asn-78	Asn-78
K_{2P}13.1 (THIK-1)	Asn-59	Asn-59	Asn-59
	Asn-65	Asn-65	Asn-65
K_{2P}15.1 (TASK-5)	No sites	No sites	No sites
K_{2P}16.1 (TALK-1)	Asn-57	Asn-57	Asn-57
	Asn-86	Asn-86	Asn-86
K_{2P}17.1 (TALK-2)	Asn-65		
	Asn-94		
K_{2P}18.1 (TRESK)	Asn-70		
	Asn-96[a]	Asn-94	Asn-83

[a] This site is predicted, but only Asn-70 is glycosylated in human K_{2P}18.1 (27).

Statistics—Graph and statistical analysis software SigmaPlot 11.0 (Systat Software, Chicago, IL) was used to plot electrophysiology data and perform significance tests. The data were first subjected to the Shapiro-Wilk test for normality. Normal populations were analyzed using Student's *t* test. Non-normal populations were analyzed using the Mann-Whitney rank sum test.

RESULTS

Glycosylation of K_{2P} Channels—Protein sequences of human, mouse, and rat K_{2P} channels were analyzed for the presence of *N*-glycosylation consensus sites using the NetNGlyc 1.0 server (21). Sites with a glycosylation potential ≥0.5 were cross-checked for predicted external domains. Thirteen of the fifteen mammalian K_{2P} channels sequenced to date contain at least one predicted glycosylation site within at least one of the three species examined (Table 2). Notably, using a threshold glycosylation potential ≥0.5, neither K_{2P}1.1 (TWIK) nor K_{2P}15.1

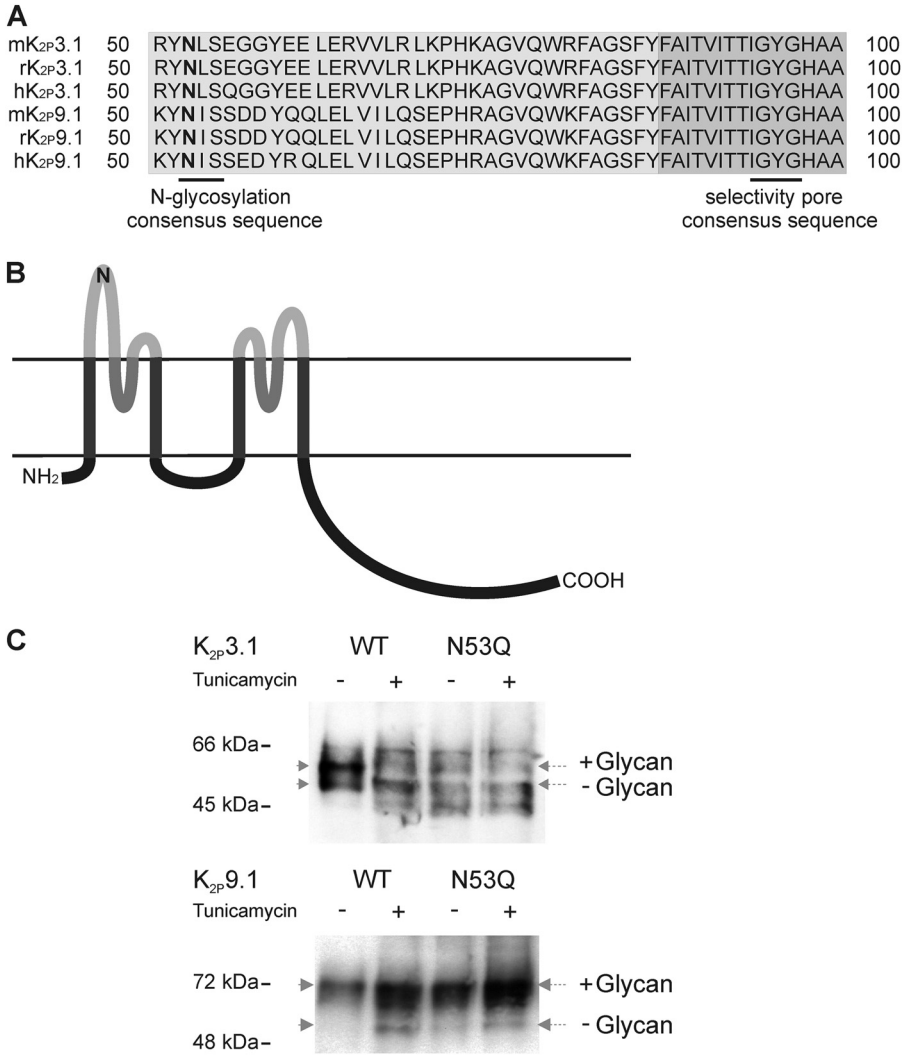

FIGURE 1. **K_{2P}3.1 and K_{2P}9.1 are glycoproteins.** *A*, partial amino acid sequence alignment of mouse, rat, and human K_{2P}3.1 and K_{2P}9.1 with *N*-linked glycosylation consensus site and channel pore selectivity sequence *highlighted*. *B*, schematic membrane topology of TASK channels subunit with four transmembrane domains (*dark gray*), pore-forming domains (*medium gray*), and external domains (*light gray*) with the location of the putative *N*-glycosylation site depicted (*N*). *C*, immunoblot showing differences in mobility of WT and glycosylation mutant (N53Q) TASK channels with or without prior treatment with tunicamycin to prevent the addition of *N*-linked glycans. Post-nuclear supernatants from untreated (−) or tunicamycin-treated (+) COS-7 cells transfected with GFP- and HA-tagged K_{2P}3.1 (*upper panel*) and K_{2P}9.1 (*lower panel*) were separated by SDS-PAGE and transferred to nitrocellulose. The membranes were probed with anti-GFP antibody (K_{2P}3.1) or anti-HA tag antibody (K_{2P}9.1). The positions of size standards are indicated on the *left*. *Dotted arrows* indicate the middle of each band.

were predicted to be glycosylated. However, K_{2P}1.1 does contain a glycosylation consensus sequence at positions 95–97 (conserved between human and rodent) with Asn-95 as a potential glycan acceptor. Lesage *et al.* (22) reported K_{2P}1.1 to be a glycoprotein, because of altered band sizes following separation by PAGE of glycopeptidase-treated channels. Significantly, K_{2P}15.1, which to date has failed to show functional expression, is the only K_{2P} channel that lacks an *N*-glycosylation consensus site (Table 2).

Both K_{2P}3.1 and K_{2P}9.1 possess a single *N*-glycosylation site at position 53 (Asn-53; rK_{2P}3.1 position potential = 0.689; rK_{2P}9.1 = 0.802). Asn-53 is located within the first external domain adjacent to the first pore and is conserved within all species examined (Fig. 1, *A* and *B*).

To determine whether Asn-53 is in fact a target for glycan attachment, we abolished the predicted glycosylation site by substitution of glutamine for asparagine, creating the mutant channels GFP-$rK_{2P}3.1_{N53Q}$HA and GFP-$rK_{2P}9.1_{N53Q}$HA. We examined whether the wild-type and glycosylation mutant channels were glycosylated when expressed in COS-7 cells. COS-7 cells transiently expressing GFP-rK_{2P}3.1-HA, GFP-$rK_{2P}3.1_{N53Q}$HA, GFP-rK_{2P}9.1-HA, and GFP-$rK_{2P}9.1_{N53Q}$HA were treated either with 1.0 μg/ml tunicamycin, which blocks synthesis of all *N*-glycans, or with its vehicle Me_2SO alone. The relative mobility of the tagged channels from total cell lysates was compared by SDS-PAGE, followed by Western blotting. For K_{2P}3.1, two distinct bands are detected in the nontreated wild-type lane; on treatment with tunicamycin or in cells transfected with GFP-$rK_{2P}3.1_{N53Q}$HA, the intensity of the upper band is decreased, whereas that of the lower band increases, suggesting a higher proportion of higher mobility channels (Fig. 1*C*). Untreated, wild-type K_{2P}9.1 channels migrate as a single band to the predicted weight. A proportion of K_{2P}9.1 from the tunicamycin-treated cells migrated further than their

untreated controls, whereas glycosylation mutant channels show mobility similar to the tunicamycin-treated wild-type channel and higher than the glycosylated wild-type channel (Fig. 1*C*).

Disruption of K_{2P}3.1 Glycosylation Prevents Channel Functional Expression—To determine whether channel glycosylation impacts channel function, we investigated the electrophysiological properties of wild-type and N53Q mutant $rK_{2P}3.1$ in HEK293 cells. The cells expressing wild-type channel show a current-voltage (*I-V*) relationship typical of K_{2P} potassium leak channels, with a reversal potential of -60.88 mV $\pm$ 3.20, ($n = 8$; Fig. 2*A*). As predicted for TASK family members, $rK_{2P}3.1$ currents were inhibited by exposure to acidic external solutions (pH 6.5) with currents at 60 mV reduced from 0.97 $\pm$ 0.17 nA at pH 7.8 to 0.45 $\pm$ 0.08 nA at pH 6.5, which is not significantly different from currents produced by untransfected cells (0.39 $\pm$ 0.09 nA at pH 7.8, $n = 8$; ($p = 0.63$); Fig. 2, *A* and *B*). HEK293 cells transiently expressing $rK_{2P}3.1_{N53Q}$ channels failed to produce current significantly different from untransfected cells at both pH 7.8 and pH 6.5 (0.41 $\pm$ 0.08 nA at pH 7.8, $n = 7$): $p = 0.81$; 0.43 $\pm$ 0.10 nA at pH 6.5 $n = 9$) and $p = 0.79$ (Fig. 2, *A* and *B*). This decrease in $rK_{2P}3.1_{N53Q}$ current compared with wild-type $rK_{2P}3.1$ current is coupled with a more positive reversal potential (-31.22 ± 6.01 mV), which is predicted if background K^+ flux is reduced.

To determine whether the observed decreased flux is due to altered channel function or a reduced number of channels on the cell surface, channel cellular localization and expression on the cell surface was investigated in COS-7 cells transiently expressing either the wild-type or glycosylation mutant $K_{2P}3.1$ channels. Channel constructs contained an internal N-terminal GFP tag plus a noninterfering HA tag incorporated into an external loop within the second pore-forming domain of the channel. The GFP tag made it possible to monitor total expression (internal and cell surface) of the wild-type and mutant channel. The external HA tag enabled quantitative comparison of the relative amount of each channel expressed at the cell surface by means of staining nonpermeablized cells with anti-HA antibodies, followed by flow cytometry (Fig. 2, *C* and *D*).

In a typical experiment, the mean surface expression level of double-tagged $rK_{2P}3.1_{N53Q}$ in live, intact cells was only 9% relative to the wild-type channel, as measured by staining externally with anti-HA tag (Fig. 2*C*; MFI values as follows: GFP-$rK_{2P}3.1$-HA, 294; GFP-$rK_{2P}3.1_{N53Q}$HA, 97; isotype control, 78). Significantly, when cells expressing double-tagged $rK_{2P}3.1$ channels were treated with 1.0 μg/ml tunicamycin, a reduction in HA tag fluorescence was observed (MFI 101), comparable with cells expressing the mutant channel. Over a series of experiments, summarized in Fig. 2*D*, disruption of glycosylation by mutation of the channel always resulted in very low cell surface expression of $K_{2P}3.1_{N53Q}$ (mean 11.3% relative to wild-type $K_{2P}3.1$; S.E. 1.1%, $n = 4$). Chemical inhibition of glycosylation by tunicamycin resulted in an average surface expression of 19.8% relative to wild-type $K_{2P}3.1$ (S.E. 4.6%, $n = 3$).

Images from immunofluorescence experiments comparing cellular localization of tunicamycin-treated and nontreated wild-type $rK_{2P}3.1$ channels together with mutant channels supported the flow cytometry data. When wild-type channels bearing both GFP and external HA tag (GFP-$rK_{2P}3.1$-HA) were transiently expressed in COS-7 cells, total channel protein expression was detected by GFP fluorescence (Fig. 2*E*, *upper panels*, *green*), whereas cell surface channel was detected using anti-HA tag antibody (*red*). GFP fluorescence is visible in all four samples: untreated and tunicamycin-treated cells expressing either wild-type and N53Q mutant $K_{2P}3.1$. Anti-HA staining, however, was only detected on the surface of untreated cells expressing wild-type channel (Fig. 2*E*, *lower panels*). Taken together these data support the conclusion that disruption of channel glycosylation has a negative effect on cell surface expression of $rK_{2P}3.1$.

External glucose concentration has been reported to impact protein glycosylation (23). We wanted to test whether reducing external glucose concentration might modulate the surface expression of $rK_{2P}3.1$. Cells transiently expressing GFP-$rK_{2P}3.1$-HA were cultured under normal cell culture glucose concentrations (4.5 g/liter or 25 mM) and reduced glucose (1.0 g/liter or 5.6 mM), and then flow cytometry (Fig. 3*A*) and confocal microscopy (Fig. 3*B*) were used to probe cell surface expression, detected by anti-HA staining. Both methods demonstrate a modest but consistent reduction in channel cell surface expression. In a typical flow cytometry experiment (Fig. 3*A*), cell surface HA tag fluorescence in cells cultured in low external glucose was 84% relative to control glucose concentrations (4.5 g/liter); over six experiments, the mean value was 88.2 $\pm$ 3.8% of the control. This reduced cell surface expression in response to reduced external glucose was not detected for the glycosylation mutant channel $rK_{2P}3.1_{N53Q}$ (Fig. 3). These data suggest that $K_{2P}3.1$ cell surface expression is linked to glucose concentration.

K_{2P}9.1 Cell Surface Expression Is Less Sensitive to Channel Glycosylation State—The impact of disrupting $rK_{2P}9.1$ glycosylation was investigated by examining the functional expression of both the wild-type and glycosylation mutant $rK_{2P}9.1$ channels by patch clamp analysis, together with examining cell surface expression of the channels by flow cytometry and immunofluorescence. Currents evoked from HEK293 cells transiently expressing either wild-type or glycosylation mutant channels showed no significant difference in channel kinetics, current amplitude, or reversal potential (Fig. 4, *A* and *B*). Reversal potential of HEK293 cells expressing $rK_{2P}9.1$ was -67.23 ± 1.31 mV ($n = 13$) compared with -60.00 ± 5.78 mV ($n = 9$) for $rK_{2P}9.1_{N53Q}$. At 60 mV test potential maximum current at pH 7.8 for wild-type channels was 2.36 $\pm$ 0.47 nA compared with 2.91 $\pm$ 0.56 nA for mutant channels ($p = 0.46$).

The mean surface expression level of GFP- and HA-tagged $rK_{2P}9.1_{N53Q}$ from three independent experiments was 63.6%, S.E. 1.7, relative to the wild-type channel, when measured by flow cytometry (Fig. 4*C*; MFI values as follows: GFP-$rK_{2P}9.1$-HA, 433; isotype control, 53; GFP-$rK_{2P}9.1_{N53Q}$HA, 287; isotype control, 52). Although there was a clear difference in MFI, there was considerable overlap between the range of fluorescence intensities of cells expressing wild-type and N53Q mutant channels. Immunofluorescence microscopy (Fig. 4*D*) also indicated a reduction in the amount of cell surface-localized GFP-$rK_{2P}9.1_{N53Q}$HA, compared with wild-type channel, but this

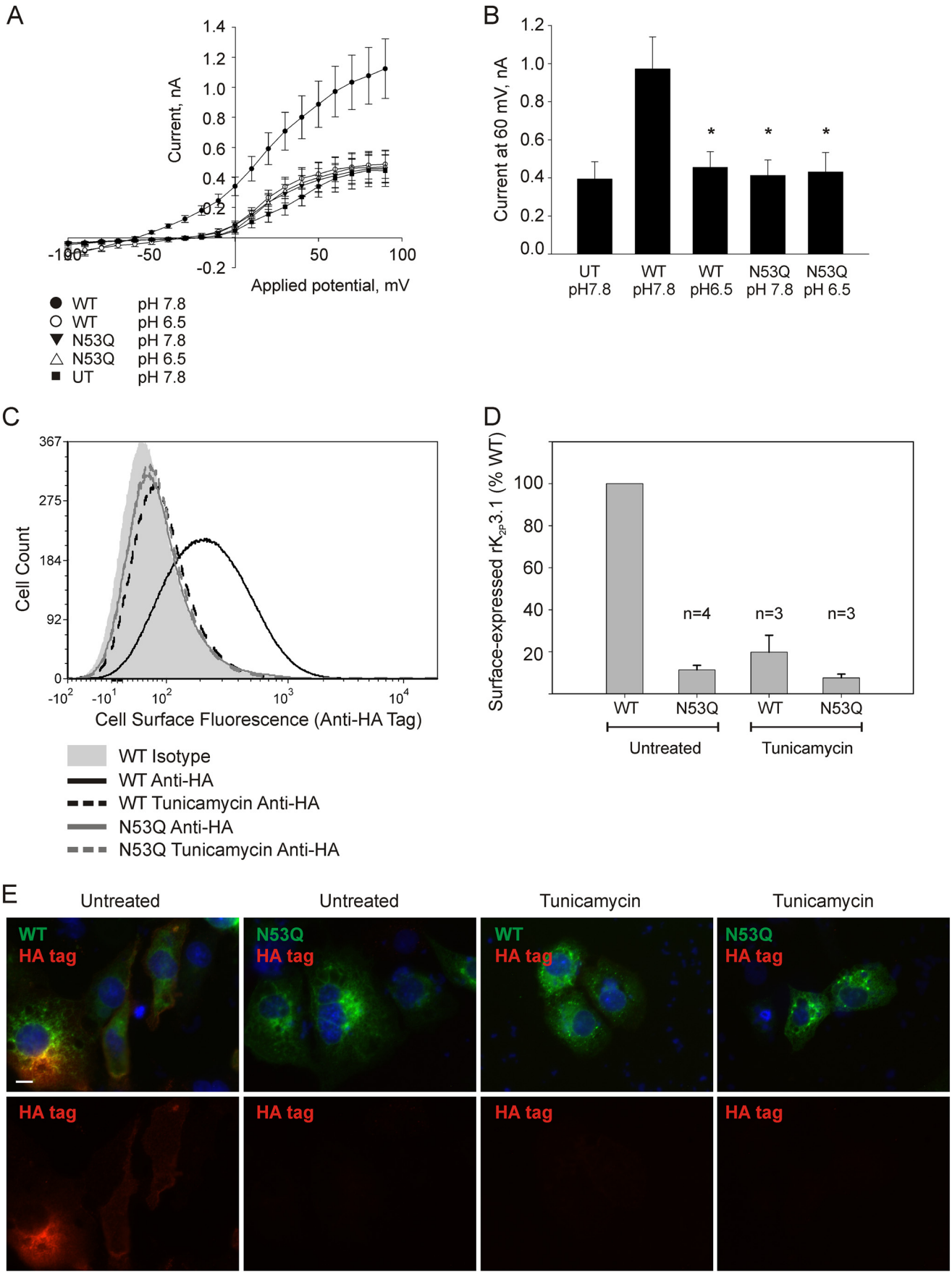
A
Current, nA
Applied potential, mV
WT pH 7.8
WT pH 6.5
N53Q pH 7.8
N53Q pH 6.5
UT pH 7.8
B
Current at 60 mV, nA
UT pH7.8
WT pH7.8
WT pH6.5
N53Q pH 7.8
N53Q pH 6.5
C
Cell Count
Cell Surface Fluorescence (Anti-HA Tag)
WT Isotype
WT Anti-HA
WT Tunicamycin Anti-HA
N53Q Anti-HA
N53Q Tunicamycin Anti-HA
D
Surface-expressed rK2P3.1 (% WT)
n=4
n=3
n=3
WT
N53Q
WT
N53Q
Untreated
Tunicamycin
E
Untreated
Untreated
Tunicamycin
Tunicamycin
WT
HA tag
N53Q
HA tag
WT
HA tag
N53Q
HA tag
HA tag
HA tag
HA tag
HA tag

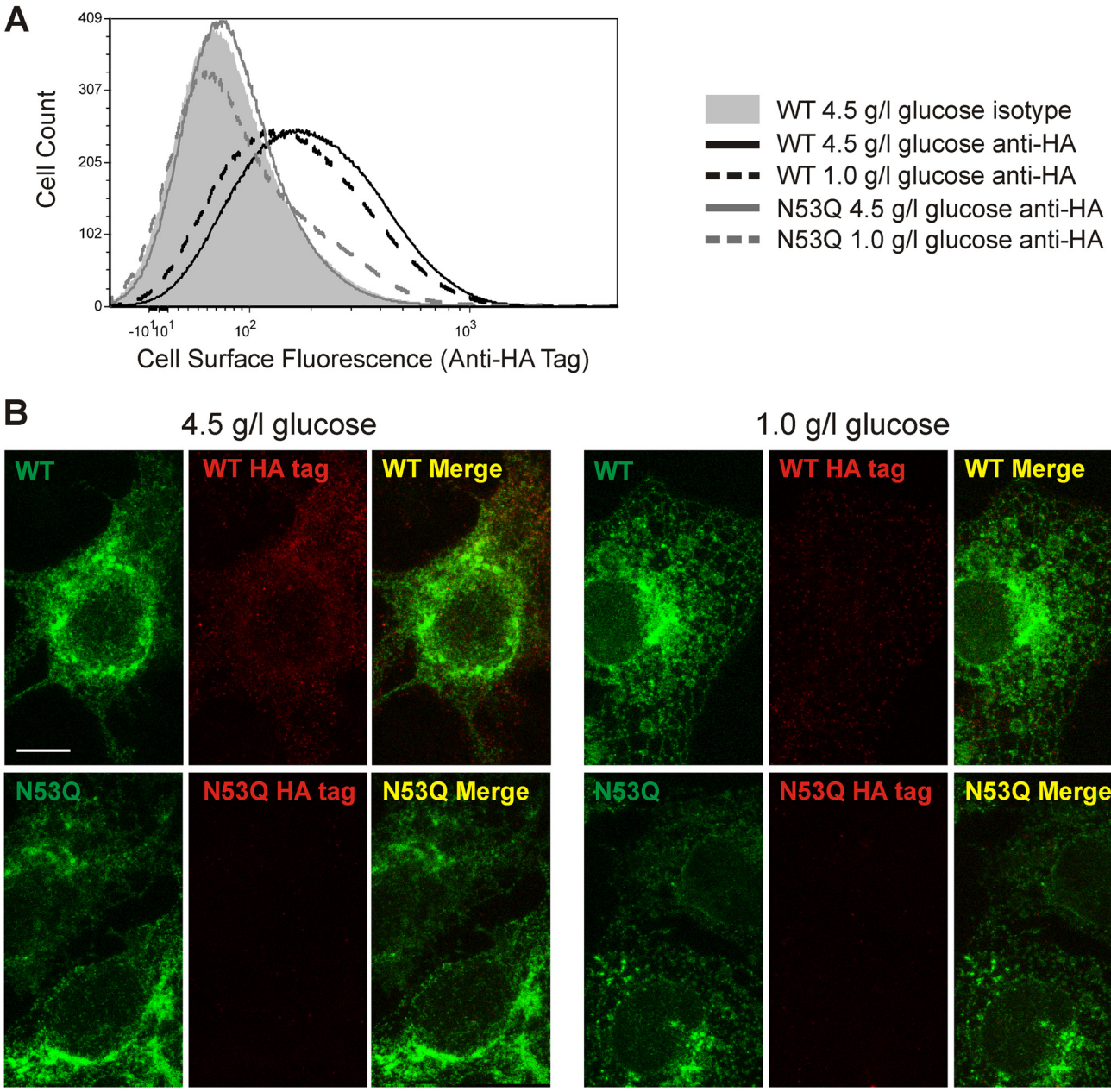

FIGURE 3. **Surface expression of $rK_{2P}3.1$ responds to a reduction in the concentration of glucose in the culture medium.** *A*, flow cytometric analysis of intact COS-7 cells expressing GFP-$rK_{2P}3.1$-HA or GFP-$rK_{2P}3.1_{N53Q}$HA. Cells were stained with either a monoclonal antibody against the external HA tag or an isotype control antibody, followed by goat anti-mouse $F(ab')_2$ fragment conjugated to Alexa Fluor 647. *Solid gray curve*, cells expressing GFP-$rK_{2P}3.1$-HA, cultured in 4.5 g/liter glucose, stained with the isotype control; *black solid line*, GFP-$rK_{2P}3.1$-HA, 4.5 g/liter glucose, anti-HA; *black dashed line*, GFP-$rK_{2P}3.1$-HA, 1.0 g/liter glucose anti-HA; *gray solid line*: GFP-$rK_{2P}3.1_{N53Q}$HA, 4.5 g/liter glucose, anti-HA; *gray dashed line*: GFP-$rK_{2P}3.1_{N53Q}$HA, 1.0 g/liter glucose, anti-HA. *B*, confocal microscopic *z*-stack images of the COS-7 cells described in *A*, fixed and stained against HA tag (*red*). *WT*, GFP-$rK_{2P}3.1$-HA; *N53Q*, GFP-$rK_{2P}3.1_{N53Q}$HA (*green fluorescence*); *Merge*, superimposed images of total channel expression (*green*) and surface-exposed HA tag (*red*). The *scale bar* represents 10 μm.

FIGURE 2. **Disruption of $rK_{2P}3.1$ glycosylation prevents channel expression.** *A*, electrophysiological properties of HEK293 cells transiently expressing $rK_{2P}3.1$ or $rK_{2P}3.1_{N53Q}$ and eGFP on separate plasmids. The *traces* were derived from at least seven cells. ●, wild-type $rK_{2P}3.1$, external pH 7.8; ○, wild-type $rK_{2P}3.1$, external pH 6.5; ▼, $rK_{2P}3.1_{N53Q}$, external pH 7.8; △, $rK_{2P}3.1_{N53Q}$, external pH 6.5; ■, untransfected cells, pH 7.8. *B*, comparison of the currents from *A* at 60 mV. *C*, representative flow cytometric analysis of intact COS-7 cells expressing GFP-$rK_{2P}3.1$-HA or GFP-$rK_{2P}3.1_{N53Q}$-HA. The cells were stained with either a monoclonal antibody against the external HA tag or an isotype control antibody, followed by goat anti-mouse $F(ab')_2$ fragment conjugated to Alexa Fluor 647. *Solid gray curve*, cells expressing GFP-$rK_{2P}3.1$-HA, stained with the isotype control; *black solid line*, cells expressing GFP-$rK_{2P}3.1$-HA and stained with anti-HA; *black dashed line*, cells expressing GFP-$rK_{2P}3.1$-HA, stained with anti-HA and treated with 1 μg/ml tunicamycin; *gray solid line*, cells expressing GFP-$rK_{2P}3.1_{N53Q}$HA and stained with anti-HA; *gray dashed line*, cells expressing GFP-$rK_{2P}3.1_{N53Q}$HA stained with anti-HA and treated with 1 μg/ml tunicamycin. *D*, comparison of the surface expression of GFP-$rK_{2P}3.1$-HA and GFP-$rK_{2P}3.1_{N53Q}$HA with or without tunicamycin treatment, from a several flow cytometric experiments. The values are percentages relative to wild-type channel in untreated cells. *E*, immunofluorescence images of fixed, nonpermeabilized COS-7 cells expressing GFP-$rK_{2P}3.1$-HA (WT) or GFP-$rK_{2P}3.1_{N53Q}$HA (N53Q), with or without tunicamycin treatment. *Upper panels*, merged GFP (*green*) and anti-HA tag-conjugated fluorescence (*red*). *Lower panels*, anti-HA tag fluorescence alone. The *scale bar* represents 10 μm.

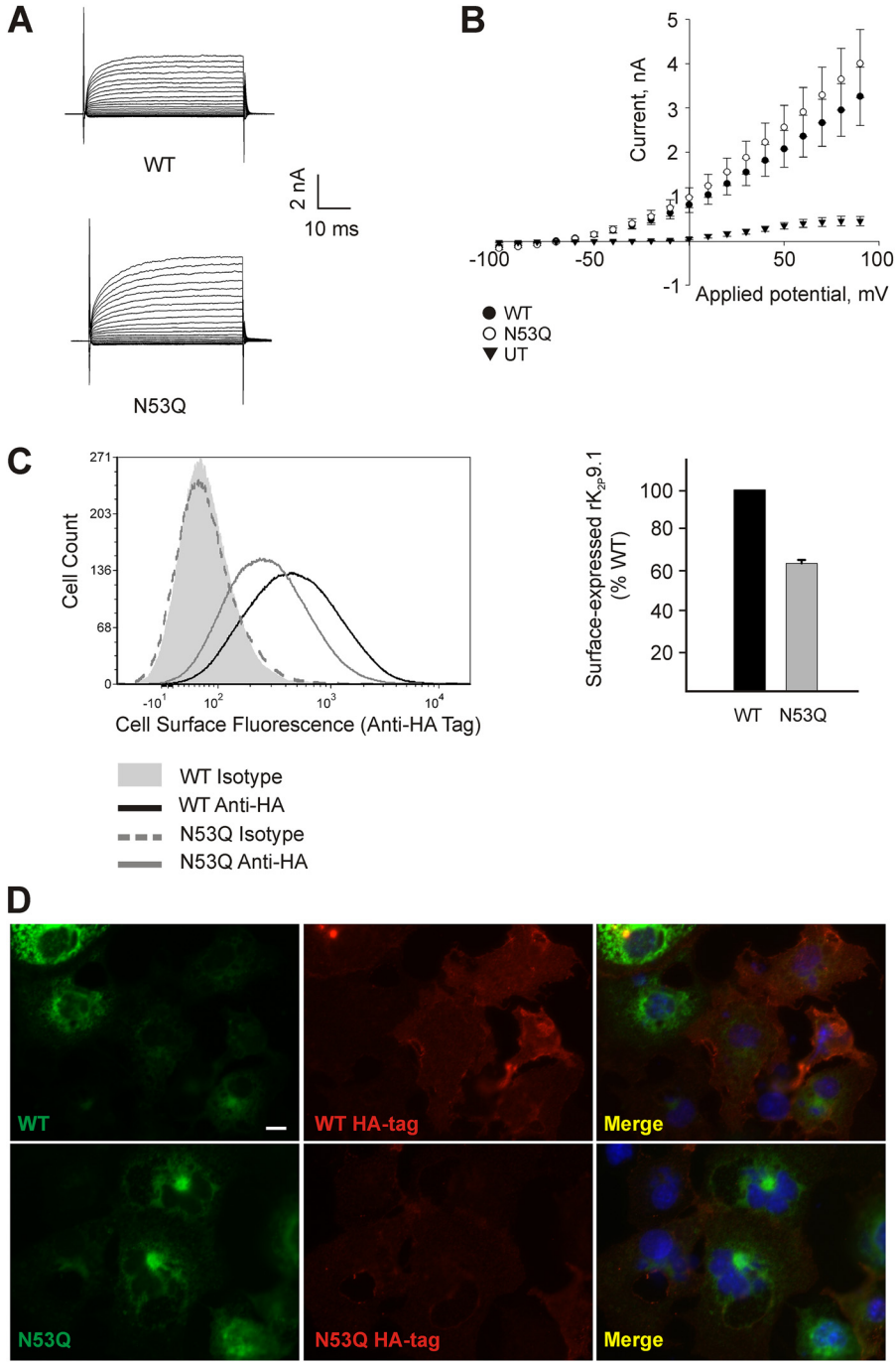

FIGURE 4. **$rK_{2P}9.1$ cell surface expression is less sensitive than $rK_{2P}3.1$ to channel glycosylation state.** *A*, currents evoked by applied membrane potential pulses from −100 to +90 mV in HEK293 cells expressing $rK_{2P}9.1$ (*WT*) or $rK_{2P}9.1_{N53Q}$ (*N53Q*) at pH 7.8. *B*, average current-voltage relationship for untransfected (*UT*) HEK293 cells, or HEK cells expressing $rK_{2P}9.1$ (*WT*) or $rK_{2P}9.1_{N53Q}$ (N53Q) at pH 7.8. *C*, flow cytometric analysis of intact COS-7 cells expressing GFP-$rK_{2P}9.1$-HA (*WT*) or GFP-$rK_{2P}9.1_{N53Q}$HA (*HA*). The cells were stained with either a monoclonal antibody against the external HA tag or an isotype control antibody, followed by goat anti-mouse $F(ab')_2$ fragment conjugated to Alexa Fluor 647. *Solid gray curve*, cells expressing GFP-$rK_{2P}9.1$-HA, stained with the isotype control. *Solid black line*, cells expressing GFP-$rK_{2P}9.1$-HA, stained with anti-HA tag antibody. *Solid gray line*, GFP-$rK_{2P}9.1_{N53Q}$HA, anti-HA-tag. *Dashed gray line*, GFP-$rK_{2P}9.1_{N53Q}$HA, isotype control. *Bar chart*, summary of three independent experiments to determine the surface expression of GFP-$rK_{2P}9.1_{N53Q}$HA (*N53Q*) to GFP-$rK_{2P}9.1$-HA (*WT*). The results are expressed relative to WT (100%). The *error bar* shows S.E. *D*, immunofluorescence images of the COS-7 cells described above, fixed and stained to detect external HA tag (*red fluorescence*). *Upper panels*, GFP-$rK_{2P}9.1$-HA; *lower panels*, GFP-$rK_{2P}9.1_{N53Q}$HA (*green fluorescence*). *Merge*, superimposed images of channel and HA tag fluorescence. The *scale bar* represents 10 μm.

reduction was less marked in comparison with GFP-$rK_{2P}3.1_{N53Q}$HA (Fig. 2*E*).

Cellular Localization of Wild-type and Glycosylation Mutant Channels—Because the nonglycosylated $rK_{2P}3.1_{N53Q}$ channel shows marked reduction in cell surface expression compared with the wild-type channel and because nonglycosylated proteins are often retarded through the secretory pathway, we asked whether the glycosylation mutant channel experienced altered trafficking to the cell surface. Previous studies have reported an ER distribution for TASK channels (7, 24). We

consistently observe a $K_{2P}3.1$ and $K_{2P}9.1$ perinuclear accumulation in transfected cells, as well as a generalized ER staining pattern, which co-localizes with an ER resident, protein disulfide isomerase. The perinuclear staining was more frequent and pronounced in the N53Q channel mutants. To characterize the subcellular localization of both the wild-type and glycosylation mutant $K_{2P}3.1$, we used markers for ERGIC (ERGIC-53) and GC (58-kDa Golgi protein). COS-7 cells transiently expressing either GFP-$rK_{2P}3.1$ or GFP-$rK_{2P}3.1_{N53Q}$ showed overlap between channel signal and each of the compartments examined (Fig. 5). To determine whether signal from the GFP-tagged channel localized specifically with signal for each of the subcellular compartments examined, the intensity of both signals (channel, *green*; and compartment, *red*) were quantified and compared along defined transects. This analysis revealed partial overlap with the 58-kDa Golgi protein for both wild-type and mutant channels (Fig. 5*A*), whereas substantial signal overlap was observed for both channels with ERGIC-53 (Fig. 5*B*). Comparable experiments were performed for $rK_{2P}9.1$ and $rK_{2P}9.1_{N53Q}$ with equivalent results (supplemental Fig. S1). Significantly, both the wild-type and glycosylation mutants for both channels were observed beyond the ER and detected in both the ERGIC and GC compartments, providing evidence that the lack of channel glycosylation does not completely block forward transport of these channels.

Does Channel Stability Contribute to Reduced Function of Glycosylation Mutant $rK_{2P}3.1_{N53Q}$?—The total expression (both intracellular and cell surface) of GFP-tagged wild-type $rK_{2P}3.1$ could be compared with the GFP-tagged N53Q mutant channel by quantitation of GFP fluorescence. In six flow cytometry experiments, the total expression of GFP-$rK_{2P}3.1_{N53Q}$-HA was reproducibly lower than the wild-type channel. In a typical experiment (Fig. 6*A*), the MFI (GFP fluorescence) of cells expressing GFP-$rK_{2P}3.1$-HA was 24,900, whereas that of GFP-$rK_{2P}3.1_{N53Q}$HA was 17,740. Tunicamycin treatment reduced the MFI of cells expressing wild-type channel to 18,400, compared with 16,460 for the N53Q mutant. We reasoned that lower total amounts of nonglycosylated channel may arise because of enhanced turnover, whether the mutant channel is targeted for degradation direct from the ER and/or is very rapidly retrieved from the plasma membrane, given that $rK_{2P}3.1_{N53Q}$ is not detected at the cell surface but does proceed through the secretory system.

Adopting a sensitive plasma membrane biotinylation method (25), we tested whether nonglycosylated $rK_{2P}3.1$ could be detected in newly formed endocytic vesicles. COS-7 cells expressing GFP-$rK_{2P}3.1$ (Fig. 6*B*, *WT panel*) or GFP-$rK_{2P}3.1_{N53Q}$ (Fig. 6*C*, *N53Q panel*) underwent cell surface biotinylation followed by a period of endocytosis. Numerous endocytic vesicles containing biotin were visible after a 20-min incubation of surface-labeled transfected cells (Fig. 6, *B* and *C*, *biotin panels*). Many of the vesicles containing biotinylated cell surface material also stained positive for the early endosome marker EEA1 (Fig. 6, *B* and *C*, *EEA1 panels*). A further subset of these vesicles was triple-stained, containing GFP-tagged wild-type or N53Q mutant channel, biotin, and EEA1 (Fig. 6, *B* and *C*, *merge panels*). The number of triple-stained vesicles for each channel was quantified, in cells transfected with wild-type $K_{2P}3.1$, 67 ± 18 ($n = 4$ fields of view) triple-stained vesicles were identified. A similar number (77 ± 19; $n = 7$) of triple-stained vesicles were identified in cells transfected with the glycosylation mutant channel. Four example transects for GFP-$rK_{2P}3.1$ and GFP-$rK_{2P}3.1_{N53Q}$ illustrate co-localization of channel, biotin, and EEA1 in individual triple-stained vesicles (numbered *1–4* in Fig. 6, *B* and *C*, *merge panels*). These results indicate that $rK_{2P}3.1_{N53Q}$ does reach the plasma membrane and, like wild-type, $rK_{2P}3.1$ is retrieved in endocytic vesicles.

DISCUSSION

Glycosylation of membrane proteins is a common post-translational modification with a variable role in the processing and function of glycoproteins (26). In this study we examined the prospect and impact of *N*-glycosylation on members of the K_{2P} family of background potassium channels with particular focus on TASK channels ($K_{2P}3.1$ and $K_{2P}9.1$) and demonstrate a conserved *N*-linked glycosylation site at Asn-53. Although membrane proteins may possess an *N*-glycosylation consensus sequence, it is worth noting that not all predicted sites undergo glycan modification. This was recently demonstrated for $K_{2P}18.1$ (or TRESK), when two sites were predicted to undergo *N*-linked glycosylation, but only one was shown to accept glycans (27). The best estimate for the proportion of all proteins glycosylated has been revised substantially downwards from over 50% to under 20% (28), underlining the importance of experimentally verifying predicted glycosylation sites. Therefore, TASK channel glycosylation was verified by electrophoresis mobility shift assays and revealed that prevention of acceptance of glycosylation alters the molecular weight and hence the mobility of these channels.

Channel glycosylation was shown to be critical for cell surface expression and hence function of $K_{2P}3.1$. Patch clamp analysis, flow cytometry, and immunofluorescence studies all verify that $K_{2P}3.1_{N53Q}$ targeting to the cell surface was disrupted. Similarly, cells transiently expressing wild-type channels treated with tunicamycin (which inhibits *N*-linked glycosylation) showed cell surface expression comparable with cells expressing the glycosylation mutant channels ($K_{2P}3.1_{N53Q}$), supporting a regulatory role for channel glycosylation in $K_{2P}3.1$ surface expression and validating that the altered surface expression is due to removal of the glycan tree rather than substitution of the Asn. Furthermore, when cells expressing wild-type $K_{2P}3.1$ were cultured in glucose concentrations lower than standard cell culture conditions, a 12% reduction in cell surface expression of $K_{2P}3.1$ was detected by flow cytometry, with reduced surface expression of the channel detected by immunofluorescence. Together, these data provide evidence that $K_{2P}3.1$ surface expression and function are sensitive to the glycosylation state of the channel.

Channel glycosylation has less impact on the surface expression and function of $K_{2P}9.1$. $K_{2P}9.1_{N53Q}$ displayed a ~40% reduction in mean surface expression when compared with the wild-type channel and quantified by flow cytometry. Channel current for wild-type and glycosylation mutant $K_{2P}9.1$ channels were not significantly different when analyzed by patch clamp analyses. These data support the conclusion that although $K_{2P}9.1$ is clearly glycosylated at Asn-

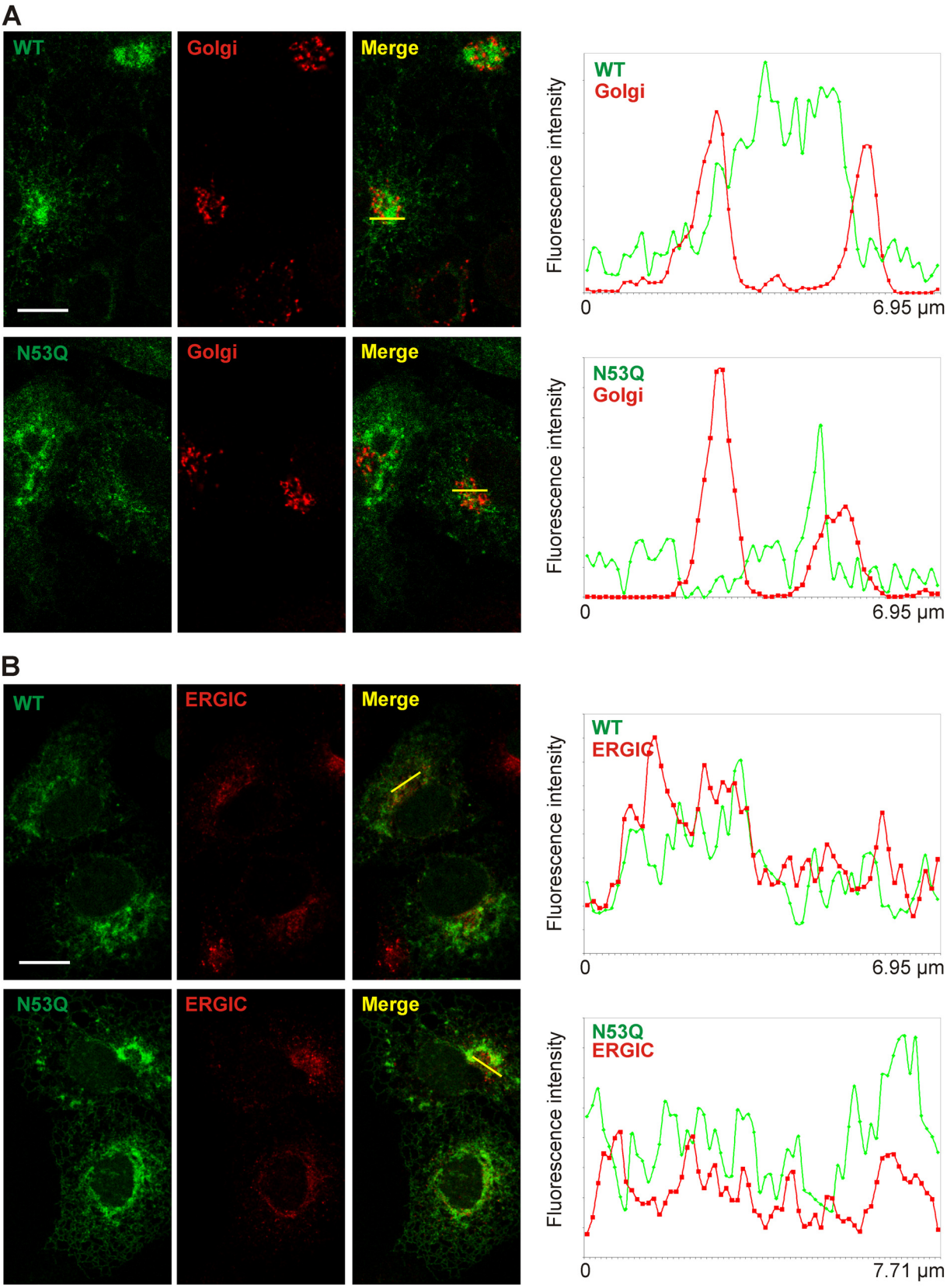

FIGURE 5. **Subcellular localization of GFP-tagged $rK_{2P}3.1$ and $rK_{2P}3.1_{N53Q}$.** *A*, COS-7 cells expressing GFP-$rK_{2P}3.1$ (*upper panels*, *WT*, *green*) or GFP-$rK_{2P}3.1_{N53Q}$ (*lower panels*, N53Q, *green*) were fixed and stained with antibodies against the 58-kDa Golgi complex protein (Golgi, *red*). *Merge*, superimposed channel and Golgi complex images. The images are single confocal sections. The *white bar* represents 10 μm. Transects in the *Merge* images (*yellow*) reveal the extent of co-localization of channel and the Golgi complex signals, because both signal intensities across the length of each transect are plotted in the graphs to the *right* of the confocal images. *B*, as *A*, but cells were stained with an antibody against ERGIC-53.

53, the lack of glycosylation at this site is not critical to the channel's surface expression and delivery and does not significantly affect channel function but has a negative impact on the overall level of channel maintained on the cell surface either by altering the efficiency of channel delivery to or removal from the cell surface.

Such a varied response of two closely related ion channels to glycosylation is not unprecedented. Indeed, members of hyper-

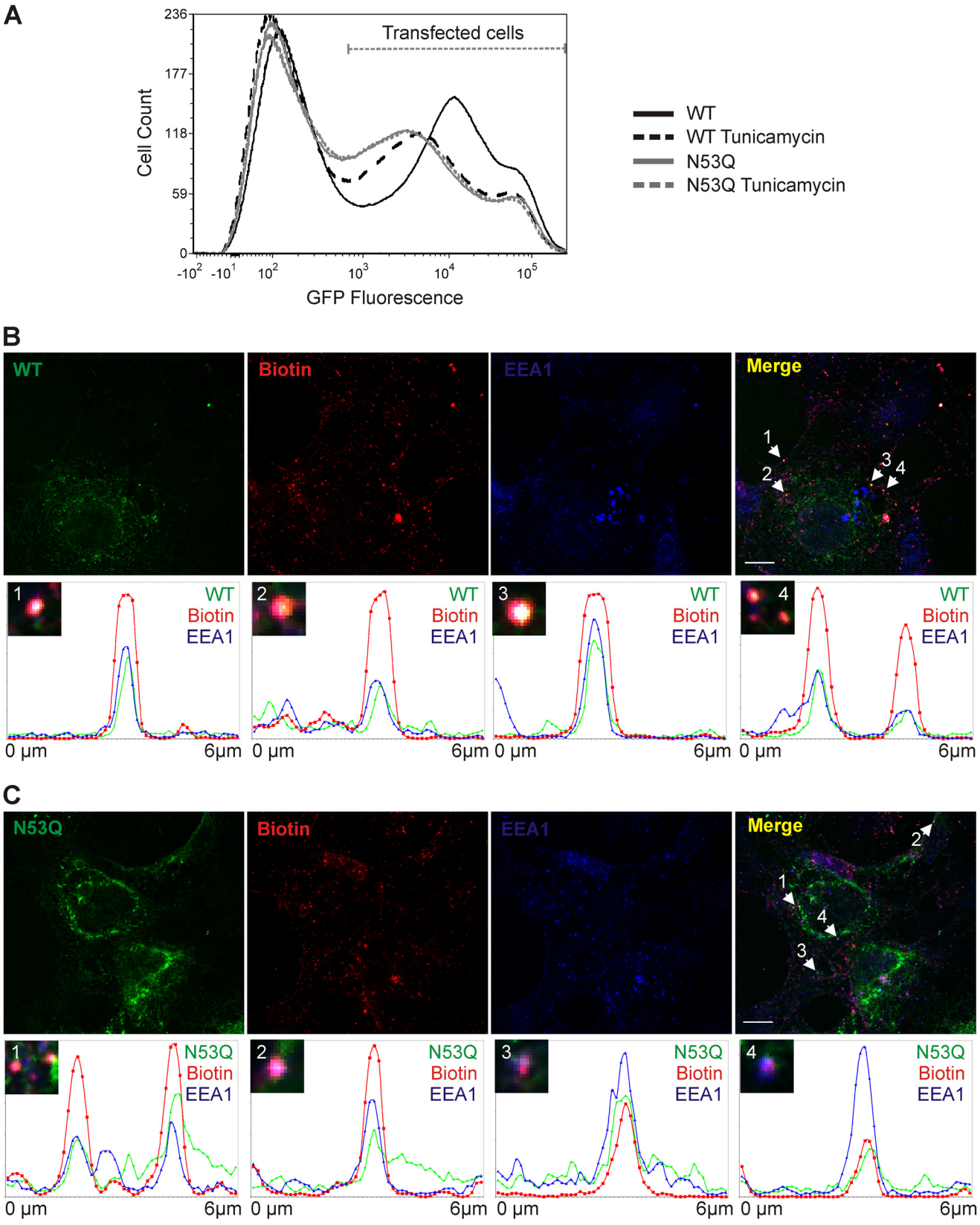

polarization-activated cyclic nucleotide-gated (HCN) channels show similar findings. HCN1 and HCN2 are both glycosylated in embryonic mouse heart (29), but whereas the surface expression of HCN2 is highly dependent on glycosylation, HCN1 is markedly less sensitive. The authors propose that the channels diverged after gene duplication from an ancestor HCN channel that did not require glycosylation for efficient cell surface localization.

The recently solved crystal structures of two K_{2P} channels: $K_{2P}1.1$ and $K_{2P}4.1$ (30, 31) were obtained using recombinant proteins from which putative glycosylation sites had been removed. The respective predicted glycosylation sites occur within a disordered region after the extracellular cap/helical cap domain and appear to be positioned away from the ion selectivity filter in each channel. We can postulate a similar arrangement for Asn-53 in $K_{2P}3.1$ and $K_{2P}9.1$, which likely places the *N*-glycan away from the channel pore and selectivity filter: in support of this, the biophysical properties of $K_{2P}9.1_{N53Q}$ did not appear to be altered when examined by whole cell patch clamp recordings.

Among their other roles, glycans have been proposed to act as targeting determinants for a number of channels, including aquaporins (AQP-2), voltage-gated potassium channels (Kv1.2), HCN channels, and acid-sensing ion channels (ASIC-1a) (29, 32–34). It is difficult, however, to discriminate between sorting *per se* and the protein quality control processes that precede targeting. The β-subunit of gastric HK-ATPase is an example of a protein where *N*-linked glycans have been shown to play a distinct role in targeting to the apical plasma membrane (35). The almost complete absence of $K_{2P}3.1_{N53Q}$ on the plasma membrane led us to investigate whether intracellular localization of the glycosylation mutant channel was disrupted.

When the intracellular localization of wild-type $K_{2P}3.1$ and mutant $K_{2P}3.1_{N53Q}$ were compared by immunofluorescence, both channels were detected in both the ERGIC and the GC. Indeed, although a degree of overlap between the GC marker and the channel was detected, substantially greater overlap between ERGIC marker and both channels was observed. Significantly, ERGIC contributes to the concentration, folding, and quality control of newly synthesized proteins. These findings are significant because they suggest that although the non-glycosylated channel is not detected on the cell surface, it does escape the ER and traffics to the ERGIC and GC. Therefore it appears that glycosylation does not in itself alter the processing pathway of $K_{2P}3.1$ channels.

If glycosylation mutant channels are not retained within the ER and pass through the secretory pathway, these channels have the possibility of two fates. Mutant channels may reach the cell surface but show lower stability and hence a higher rate of turnover, or they may be targeted directly for degradation. Because *N*-linked glycosylation of $K_{2P}3.1$ channels does not appear to alter intracellular transport of the channel, we sought to determine whether glycosylation had an impact on channel turnover. By flow cytometry, a reduction in the total (intracellular and cell surface) amount of $K_{2P}3.1_{N53Q}$ per cell compared with the wild type was observed. Similarly, tunicamycin-treated cells expressing $K_{2P}3.1$ showed a similar reduction, with total channel per cell comparable with ablation of the glycosylation site. These observations are significant when considered together with our recycling data. When channel retrieval from the cell surface and entry into the endocytic pathway is studied, although $K_{2P}3.1_{N53Q}$ is not detected on the cell surface, $K_{2P}3.1_{N53Q}$ which was tagged by surface labeling with biotin (and therefore must have reached the cell surface) is detected within the endocytic pathway. Together these data suggest that although $K_{2P}3.1$ cannot be detected at the cell surface, a proportion of the channel population does reach the plasma membrane but is retrieved and likely targeted for degradation via the endocytic pathway. These studies provide strong evidence that channel glycosylation plays an important role in the stability of $K_{2P}3.1$ expression on the cell surface.

How Might Glycosylation Contribute to the Stability of $K_{2P}3.1$ Once Delivered to the Plasma Membrane?—The two glycans on wild-type CFTR have been shown to promote proper apical recycling; in their absence, CFTR is more rapidly internalized and is targeted to the basolateral membrane, where it appears to have a shorter half-life than glycosylated CFTR (36). The same glycans also play a role in the stability of the channel once it has exited the ER (36). A subset of the *N*-glycans attached to the HK-ATPase β is responsible for delivery of the protein to the apical membrane and retaining it there (35). It has been suggested that extracellular lectins may play a role in binding HK-ATPase and stabilizing it at the cell surface (37). Glycosylation increases thermodynamic stability by reducing the amount of surface area accessible to solvent, which in turn influences structural dynamics and protein function (26); this effect has been clearly demonstrated for the thermostability of human aquaporin 10 protein (39). Although a number of potential mechanisms exist, it will be important to find out how glycosylation contributes to the stability of $K_{2P}3.1$ and to determine the process that renders $K_{2P}9.1$ less sensitive to this regulation.

TASK channels are expressed in both neuronal and cardiac cell populations and significantly have been identified in glucose-sensing neurons of the hypothalamus, as well as peripheral specialized chemo- and nutrient-sensing cells (40, 41). Sensitivity of $K_{2P}3.1$ cell surface expression and turnover to its glycosylation state represents a potential link between metabolic status and cellular activity. Down-regulation of TASK channels is known to influence cellular depolarization. Hence, decreased cell surface expression of $K_{2P}3.1$ channels in

FIGURE 6. **Is reduced function of glycosylation mutant $rK_{2P}3.1_{N53Q}$ caused by lower channel stability?** *A*, flow cytometric analysis of COS-7 cells expressing GFP-$rK_{2P}3.1$-HA without (*solid black line*) and in the presence of 1 μg/ml tunicamycin (*dashed black line*) or GFP-$rK_{2P}3.1_{N53Q}$HA without (*solid gray line*) or with tunicamycin (*dashed gray line*). The population of GFP-positive cells is denoted by *Transfected cells*, derived by comparing with cells transfected with empty vector alone (data not shown). *B*, *upper panels*, confocal microscopic images of COS-7 cells transfected with GFP-$rK_{2P}3.1$ (*WT*, *green*), surface biotinylated (Biotin, *red*), and then allowed to endocytose for 20 min before fixing and staining with anti-EEA1 (EEA1, *blue*). *Merge*, superimposed images of channel, biotin and EEA1. Examples of triple-stained vesicles are denoted with *white arrows*, and the *numbers* correspond to transects (transects themselves not shown on the *Merge* image), which appear in the *lower panels 1–4*, as graphs of fluorescence intensity against distance. The *white scale bar* represents 10 μm. *C*, as described for *B*, except cells express GFP-$rK_{2P}3.1_{N53Q}$ (N53Q, *green*).

response to decreased glucose would lead to increased neuronal excitation. Furthermore, in the diabetic patient, with sustained higher blood glucose levels, one would predict that this environment would promote $K_{2P}3.1$ channel surface expression with resultant dampening of cellular activity.

The importance of the findings presented in this study lies in the numerous roles TASK channels may play in cellular regulation. Their varied sensitivity and stability to glycosylation, and by association glucose concentration, opens a host of potential regulatory pathways in which these important channels may be involved.

Acknowledgments—We are grateful to Dr. David Johnston of the University of Southampton Biomedical Imaging Unit for assistance with confocal microscopy, Kelly Wilkinson for expert technical support, and Prof. Stephen High at the University of Manchester for helpful comments.

REFERENCES

1. Goldstein, S. A., Bockenhauer, D., O'Kelly, I., and Zilberberg, N. (2001) Potassium leak channels and the KCNK family of two-P-domain subunits. *Nat. Rev. Neurosci.* **2,** 175–184
2. Lotshaw, D. P. (2007) Biophysical, pharmacological, and functional characteristics of cloned and native mammalian two-pore domain K^+ channels. *Cell Biochem. Biophys.* **47,** 209–256
3. Enyedi, P., and Czirják, G. (2010) Molecular background of leak K^+ currents. Two-pore domain potassium channels. *Physiol. Rev.* **90,** 559–605
4. Buckler, K. J., Williams, B. A., and Honore, E. (2000) An oxygen-, acid- and anaesthetic-sensitive TASK-like background potassium channel in rat arterial chemoreceptor cells. *J. Physiol.* **525,** 135–142
5. Patel, A. J., Honoré, E., Lesage, F., Fink, M., Romey, G., and Lazdunski, M. (1999) Inhalational anesthetics activate two-pore-domain background K^+ channels. *Nat. Neurosci.* **2,** 422–426
6. Sirois, J. E., Lei, Q., Talley, E. M., Lynch, C., 3rd, and Bayliss, D. A. (2000) The TASK-1 two-pore domain K^+ channel is a molecular substrate for neuronal effects of inhalation anesthetics. *J. Neurosci.* **20,** 6347–6354
7. O'Kelly, I., Butler, M. H., Zilberberg, N., and Goldstein, S. A. (2002) Forward transport. 14-3-3 binding overcomes retention in endoplasmic reticulum by dibasic signals. *Cell* **111,** 577–588
8. Rajan, S., Preisig-Muller, R., Wischmeyer, E., Nehring, R., Hanley, P. J., Renigunta, V., Musset, B., Schlichtorl, G., Derst, C., Karschin, A., and Daut, J. (2002) Interaction with 14-3-3 proteins promotes functional expression of the potassium channels TASK-1 and TASK-3. *J. Physiol.* **545,** 13–26
9. O'Kelly, I., and Goldstein, S. A. (2008) Forward transport of $K_{2P}3.1$. Mediation by 14-3-3 and COPI, modulation by p11. *Traffic* **9,** 72–78
10. Mant, A., Elliott, D., Eyers, P. A., and O'Kelly, I. M. (2011) Protein kinase A is central for forward transport of two-pore domain potassium channels $K_{2P}3.1$ and $K_{2P}9.1$. *J. Biol. Chem.* **286,** 14110–14119
11. Delisle, B. P., Anson, B. D., Rajamani, S., and January, C. T. (2004) Biology of cardiac arrhythmias. Ion channel protein trafficking. *Circ. Res.* **94,** 1418–1428
12. Mathie, A., Rees, K. A., El Hachmane, M. F., and Veale, E. L. (2010) Trafficking of neuronal two pore domain potassium channels. *Curr. Neuropharmacol.* **8,** 276–286
13. Gong, Q., Anderson, C. L., January, C. T., and Zhou, Z. (2002) Role of glycosylation in cell surface expression and stability of HERG potassium channels. *Am. J. Physiol.* **283,** 77–84
14. Helenius, A., and Aebi, M. (2004) Roles of *N*-linked glycans in the endoplasmic reticulum. *Annu. Rev. Biochem.* **73,** 1019–1049
15. Cohen, D. M. (2006) Regulation of TRP channels by *N*-linked glycosylation. *Semin. Cell Dev. Biol.* **17,** 630–637
16. Hall, M. K., Cartwright, T. A., Fleming, C. M., and Schwalbe, R. A. (2011) Importance of glycosylation on function of a potassium channel in neuroblastoma cells. *PLoS One* **6,** e19317
17. Schwarz, F., and Aebi, M. (2011) Mechanisms and principles of *N*-linked protein glycosylation. *Curr. Opin. Struct. Biol.* **21,** 576–582
18. Aebi, M., Bernasconi, R., Clerc, S., and Molinari, M. (2010) *N*-Glycan structures. Recognition and processing in the ER. *Trends Biochem. Sci.* **35,** 74–82
19. Appenzeller-Herzog, C., and Hauri, H. P. (2006) The ER-Golgi intermediate compartment (ERGIC). In search of its identity and function. *J. Cell Sci.* **119,** 2173–2183
20. Kamiya, Y., Satoh, T., and Kato, K. (2012) Molecular and structural basis for *N*-glycan-dependent determination of glycoprotein fates in cells. *Biochim. Biophys. Acta.* **1820,** 1327–1337
21. Blom, N., Sicheritz-Pontén, T., Gupta, R., Gammeltoft, S., and Brunak, S. (2004) Prediction of post-translational glycosylation and phosphorylation of proteins from the amino acid sequence. *Proteomics* **4,** 1633–1649
22. Lesage, F., Guillemare, E., Fink, M., Duprat, F., Lazdunski, M., Romey, G., and Barhanin, J. (1996) TWIK-1, a ubiquitous human weakly inward rectifying K^+ channel with a novel structure. *EMBO J.* **15,** 1004–1011
23. Hayter, P. M., Curling, E. M., Baines, A. J., Jenkins, N., Salmon, I., Strange, P. G., Tong, J. M., and Bull, A. T. (1992) Glucose-limited chemostat culture of Chinese hamster ovary cells producing recombinant human interferon-gamma. *Biotechnol. Bioeng.* **39,** 327–335
24. Renigunta, V., Yuan, H., Zuzarte, M., Rinné, S., Koch, A., Wischmeyer, E., Schlichthörl, G., Gao, Y., Karschin, A., Jacob, R., Schwappach, B., Daut, J., and Preisig-Müller, R. (2006) The retention factor p11 confers an endoplasmic reticulum-localization signal to the potassium channel TASK-1. *Traffic* **7,** 168–181
25. Richardson, D. S., and Mulligan, L. M. (2010) Direct visualization of vesicle maturation and plasma membrane protein trafficking. *J. Fluoresc.* **20,** 401–405
26. Solá, R. J., Rodríguez-Martínez, J. A., and Griebenow, K. (2007) Modulation of protein biophysical properties by chemical glycosylation. Biochemical insights and biomedical implications. *Cell Mol. Life Sci.* **64,** 2133–2152
27. Egenberger, B., Polleichtner, G., Wischmeyer, E., and Döring, F. (2010) *N*-Linked glycosylation determines cell surface expression of two-pore-domain K^+ channel TRESK. *Biochem. Biophys. Res. Commun.* **391,** 1262–1267
28. Khoury G. A., Baliban R. C., and Floudas C. A. (2010) Proteome-wide post-translational modification statistics. Frequency analysis and curation of the Swiss-Prot database. *Sci. Rep.* **1,** 90
29. Hegle, A. P., Nazzari, H., Roth, A., Angoli, D., and Accilli, E. A. (2010) Evolutionary emergence of *N*-glycosylation as a variable promoter of HCN channel surface expression. *Am. J. Physiol.* **298,** C1066–C1076
30. Miller, A. N., and Long, S. B. (2012) Crystal structure of the human two-pore domain potassium channel K2P1. *Science* **335,** 432–436
31. Brohawn, S. G., del Mármol, J., and MacKinnon, R. (2012) Crystal structure of the human K2P TRAAK, a lipid- and mechano-sensitive K^+ ion channel. *Science* **335,** 436–441
32. Zhu, J., Recio-Pinto, E., Hartwig, T., Sellers, W., Yan, J., and Thornhill, W. B. (2009) The Kv1.2 potassium channel. The position of an *N*-glycan on the extracellular linkers affects its protein expression and function. *Brain Res.* **1251,** 16–29
33. Moeller, H. B., Olesen, E. T., and Fenton, R. A. (2011) Regulation of the water channel aquaporin-2 by posttranslational modification. *Am. J. Physiol.* **300,** F1062–F1073
34. Jing, L., Chu, X. P., Jiang, Y. Q., Collier, D. M., Wang, B., Jiang, Q., Snyder, P. M., and Zha, X.-M. (2012) *N*-Glycosylation of acid-sensing ion channel 1a regulates its trafficking and acidosis-induced spine remodeling. *J. Neurosci.* **32,** 4080–4091
35. Vagin, O., Turdikulova, S., and Sachs, G. (2004) The H,K-ATPase β subunit as a model to study the role of *N*-glycosylation in membrane trafficking and apical sorting. *J. Biol. Chem.* **279,** 39026–39034
36. Cholon, D. M., O'Neal, W. K., Randell, S. H., Riordan, J. R., and Gentzsch, M. (2009) Modulation of endocytic trafficking and apical stability of CFTR in primary human airway epithelial cultures. *Am. J. Physiol.* **298,** L304–L314
37. Chang, X. B., Mengos, A., Hou, Y. X., Cui, L., Jensen, T. J., Aleksandrov, A., Riordan, J. R., and Gentzsch, M. (2008) Role of *N*-linked oligosaccharides

in the biosynthetic processing of the cystic fibrosis membrane conductance regulator. *J. Cell Sci.* **121,** 2814–2823
38. Deleted in proof
39. Öberg, F., Sjöhamn, J., Fischer, G., Moberg, A., Pedersen, A., Neutze, R., and Hedfalk, K. (2011) Glycosylation increases the thermostability of human aquaporin 10 protein. *J. Biol. Chem.* **286,** 31915–31923
40. Duprat, F., Lauritzen, I., Patel, A., and Honoré, E. (2007) The TASK background K_{2P} channels. Chemo- and nutrient sensors. *Trends Neurosci.* **30,** 573–580
41. O'Kelly, I., Stephens, R. H., Peers, C., and Kemp, P. J. (1999) Potential identification of the O_2-sensitive K^+ current in a human neuroepithelial body-derived cell line. *Am. J. Physiol.* **276,** L96–L104